Fabrication and Characterization of Asymmetric Janus and Ternary Particles

Chien-Chih Lin, Chu-Wei Liao, Yi-Cheng Chao, and Changshu Kuo*

Department of Materials Science and Engineering, National Cheng Kung University, Tainan 701-01, Taiwan

ABSTRACT Asymmetric Janus and ternary silica particles with an average diameter of 450 nm were fabricated by sequentially arranged particle-embedding and surface-modification processes. Thermally induced embedding of particles into polymer-fiber substrates allowed for precise control of the degree of particle submergence and the subsequent chemical modification of the hemispherical exposed particle surfaces. In addition to Janus particles with the desired surface-functionality ratios of 1:2, 1:1, and 2:1, this unique fabrication approach was also used to produce complicated and well-defined heterogeneous materials, including bifunctionalized Janus and ternary particles. The bifunctionalized Janus particles were produced with two hemispherical surfaces alternately labeled with gold and iron oxide nanoparticles, which simultaneously enabled anisotropic surface-plasmon resonance and a magnetic response. Ternary particles were also constructed, yielding submicrometer spheres with functionalized equatorial belts. The surface distributions of functional components in these spherical materials were carefully examined for uniformities in particle embedding. Statistical analyses revealed that the functional components were distributed with a uniformity of over 80% for all of the asymmetric Janus and ternary particles.

KEYWORDS: Janus particles • ternary particles • asymmetric • bifunctionalized • nanomaterials

INTRODUCTION

Low-dimensional structures and nanoscale materials with heterogeneous and asymmetric compositions have recently attracted growing interest in diverse research fields for a wide variety of applications. Distinguishing these materials from homogeneous nanomaterials, these unique substances not only preserve the variety and superiority of nanoscale properties but also exhibit great potential for definable manipulations and anisotropic performance. Among these candidates, Janus particles and Janus-like materials have received the most attention in recent years (1, 2). Janus particles are typically constructed of two distinct hemispheres with spatially distributed compositions that can differ in either their chemical functionalities or their geometric structures.

In most cases, fabrication approaches and selected core materials determine the size and characteristics of Janus particles. For example, the direct dual-supply method involves the formation of biphasic droplets from a mixture of two immiscible liquid materials (2, 3). This method enables the mass production of Janus particles with diameters of tens of micrometers. Alternatively, ready-made silica or polystyrene particles with diameters ranging from several hundreds of nanometers to a few micrometers have been extensively adapted as cores in template-assisted fabrication methods (4−8). Partial particle embedding or shielding directs the subsequent modifications only to the selected hemispherical surfaces. Janus-like heterogeneous materials, which can be as small as only a few nanometers, are often referred to as Janus micelles or Janus dendrimers. The former are based on block copolymers (9−11) or the uneven emulsification of nanoparticles (NPs) by two types of surfactants or ligands (12), whereas the latter are synthesized by the assembly of two dendritic moieties on opposite sides of the core molecules (13).

The extensive studies and applications of these Janus materials have been largely inspired by their multiple functionalities and spatial asymmetry. For instance, an ionically charged hemisphere can yield a particle rotation driven by an electric field, with potential applications in bistable displays (14, 15). The alignment of magnetic Janus particles under an external magnetic field also reveals their anisotropic ferromagnetic behavior (16−18). Anisotropic image probes have been achieved by the use of fluorescently labeled Janus particles (19, 22). The assembly of Janus-like materials has been simulated (20, 21) and experimentally realized using pH-sensitive ionic functionalities (23) or specific chemical affinities (24) located on the particle surfaces.

The success of these approaches relies on the highly uniform spatial distribution of heterogeneous characteristics. The uniform distribution of functional components and precise compositional control in a confined geometry become even more essential in the case of scaled-down or more complicated heterogeneous materials such as ternary particles (25). However, the synthesis of scaled-down materials and delicate heterogeneous characteristics usually compromises uniformity. Research trends and demands in this area thus require fabrication methods that simultaneously achieve uniform and controllable distributions of functional components while reducing the size of heterogeneous materials to submicrometer or nanometer scales.

Our previous study (26) reported the fabrication of symmetric 50/50 Janus particles with submicrometer silica-

* To whom correspondence should be addressed. E-mail: changshu@mail.ncku.edu.tw.

Received for review July 27, 2010 and accepted October 13, 2010

DOI: 10.1021/am1006589

sphere cores by 50% particle embedding and gas-phase silanization of the exposed hemisphere surface. Particle adsorption and embedding were efficiently carried out over a large surface area of electrospun polymer microfibers consisting of two glassy polymers, poly(methyl methacrylate) (PMMA) and poly(4-vinylpyridine) (P4VP). It has been estimated that about 10^9 Janus particles were fabricated from 1 mg of polymer-fiber mats (26). The laboratory production scale easily reached 10−100 mg of Janus particles in one batch. The utility of the temperature-dependent interfacial tension of these fibers with silica particles as well as the steady and uniform degree of particle submergence obtained with isothermal treatment was demonstrated.

In the current work, the Janus particle fabrication process was further modified to produce asymmetric binary Janus and ternary particles with uneven surface-functionality distributions. Manipulating the isothermal temperature allowed for the precise control of silica particle submergence to the levels of one-third or two-thirds, thus producing asymmetric Janus particles with 2:1 and 1:2 hemispheric ratios. The desired degrees of particle embedding and surface modifications were also sequentially rearranged to produce more complicated and well-designed heterogeneous nanomaterials including "Saturn-like" ternary particles and bifunctionalized Janus particles. The ternary particles with functionalized equatorial belts (27) crossing the middle of the silica particles were fabricated by sequential two-step embeddings, one surface-modification process, and one surface-etching process. This middle section is a belt of about 150 nm wide that circles the submicrometer particle and separates the two polar caps. The preparation of bifunctionalized Janus particles, in contrast, was initiated by the embedding of prefunctionalized silica particles followed by one etching process and one surface modification. As a preliminary demonstration, a bifunctionalized Janus particle was constructed with two hemispherical surfaces alternately labeled with gold (Au) and iron oxide (Fe_3O_4) NPs. The anisotropic surface-plasmon resonance (SPR) and the magnetically driven manipulation of these particles were also investigated.

Conventional two-dimensional imaging techniques provided limited observations of the three-dimensional distribution of functional components on the spherically curved surfaces. Therefore, the distributions of functional components in the Janus and ternary particles and their uniformities were examined indirectly by conducting scanning electron microscopy (SEM) of the hemispherical surfaces of the embedded particles. In the case of the half- and two-thirds-embedded particles, the diameters of the exposed hemispheres were statistically measured and converted to the upper-hemisphere surface areas. For one-third-embedded silica samples, an additional particle detachment was used to quantify the diameters of the crater edges, which represented the size and uniformity of the submerged hemisphere surfaces. Statistical analyses of the one-third-, half-, and two-thirds-submerged silica particles showed that the uniformities of the specific surface areas were all above 80%, indicating that the Janus and ternary particles had similar uniformities of the distribution of functional components and surface characteristics.

EXPERIMENTAL SECTION

Materials. Polymer microfibers serving as the particle-embedding substrates were electrospun from a solution containing poly(methyl methacrylate) and poly(4-vinylpyridine) (PMMA/P4VP, 1:1 by weight). The electrospinning process and solution formula were as previously reported (26). Solvents, including *N*, *N*-dimethylformamide and methyl ethyl ketone (MEK), were dried with anhydrous $MgSO_4$ prior to use. The aminosilane, (3-aminopropyl)trimethoxysilane (3-APTMS), was used for the particle-surface silanization via a chemical-vapor-deposition (CVD) process. Silica particles (Alfa Aesar) with an average diameter of 450 nm were precleaned by sonication in a NaOH/ethanol solution followed by centrifugal separation and eight washings with deionized (DI) water. Au and Fe_3O_4 NPs were employed for the labeling of amino-enriched silica surfaces. Au NPs with diameters of about 10 nm were synthesized by the reduction of $HAuCl_4$ in the presence of $NaBH_4$ (26). Fe_3O_4 NPs of about 15 nm diameter were prepared by the chemical coprecipitation of ferrous ($FeCl_2$) and ferric ($FeCl_3$) salts in an alkaline solution, followed by their dispersion in an aqueous solution of sodium citrate for subsequent surface modification (28).

The fabrication of asymmetric Janus and ternary particles followed basically the same procedure as that of the 50/50 Janus particles (sample JP-1-1) (26). The preparation procedures were slightly modified and consisted of four individual steps:

Particle Adsorption. The adsorption of silica particles onto the polymer-fiber surfaces was initiated by the dipping of 10 mg of PMMA/P4VP fiber mats into 20 mL of an aqueous silica suspension (pH = 6; about 1 wt % silica content). The suspension was sonicated for a few seconds to eliminate trapped air bubbles. After 10 min of dipping, moderate rinses with DI water removed the excess particles with no direct attachment to fiber surfaces. The polymer fibers and adsorbed silica particles were then dried under vacuum at room temperature.

Particle Embedding. Because the PMMA/P4VP polymer blend has two separate glass transition temperatures (120 and 140 °C), the surface tension between silica particles and thermally softened fiber substrates balances the temperature-dependent particle submergence. As a result, 4-h isothermal treatments at 120, 135, and 150 °C yielded one-third-, half-, and two-thirds-submerged silica particles, respectively, in the fiber substrates.

Surface Modification. Surface modifications of the silica particles were achieved by an aminosilane CVD process. A silane atmosphere produced from about 0.1 mL of 3-APTMS was introduced into a 500 mL vacuum chamber in which the polymer-fiber mats with embedded silica particles were held at 90 °C. After the CVD process, the vacuum chamber was incubated at the same temperature for 1 h more to ensure completion of the silanization reaction. The amino-enriched silica surfaces were later labeled with NPs by dipping the fiber mats into an aqueous suspension of Au NPs or citrate-modified Fe_3O_4 NPs. In a separate experiment, silica particles were fully functionalized with amino groups via a liquid-phase silanization. To 50 mL of anhydrous ethanol containing 2 wt % 3-APTMS were added 50 mg of precleaned silica particles, and the reaction was held for 24 h at room temperature with mild stirring.

Surface Etching. Bifunctionalized Janus and ternary particles were also fabricated using a surface-etching process. The exposed amino-enriched hemispheres of the embedded silica particles with Au NPs were etched with an aqueous NaOH solution (5 wt %) at room temperature. The PMMA/P4VP fiber mats remained intact, whereas the basic etching solution

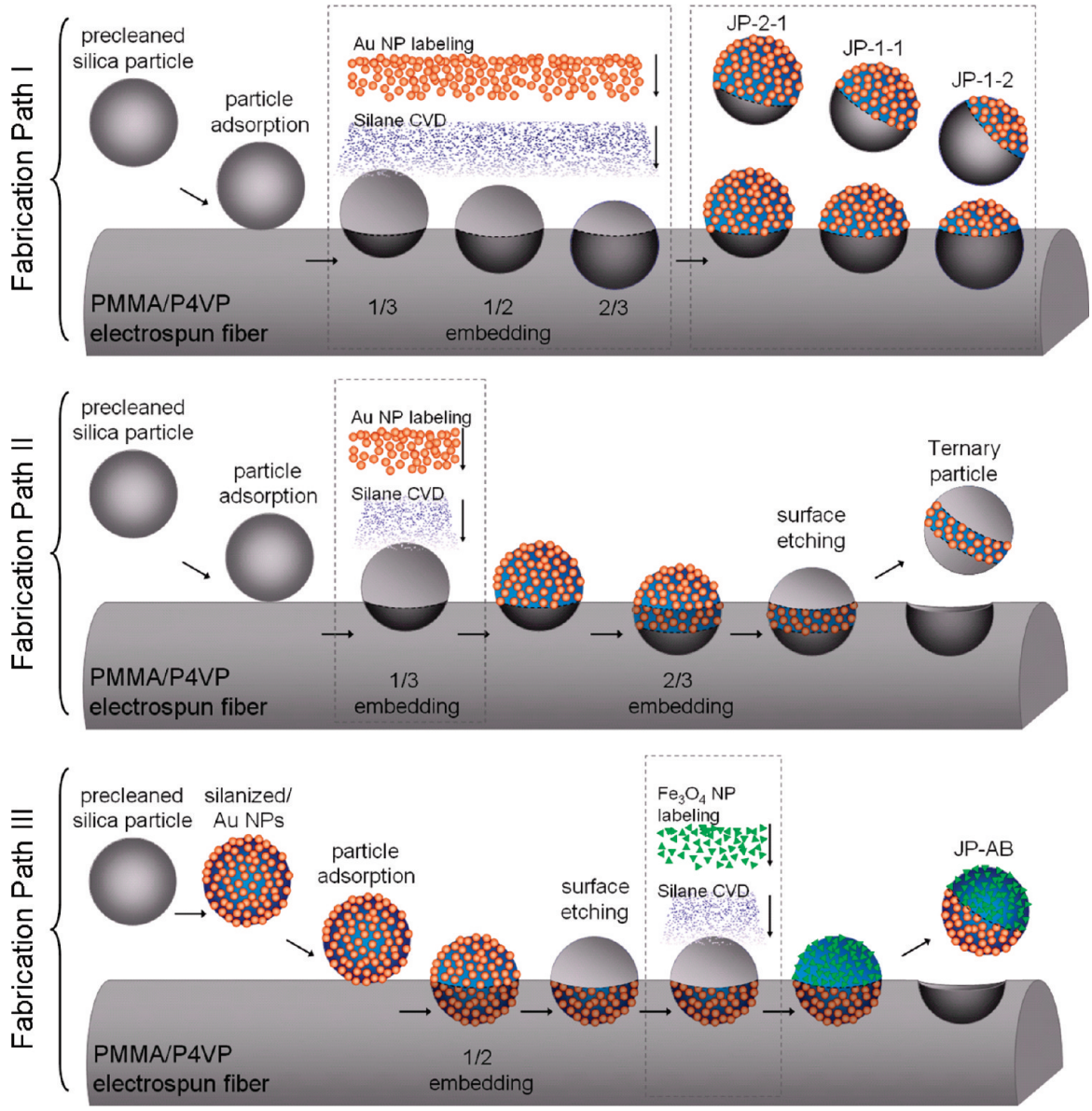

FIGURE 1. Three fabrication paths for (I) three kinds of asymmetric Janus particles, (II) ternary particles, and (III) bifunctionalized Janus particles.

detached the aminosilane layer and regenerated a flesh silica surface for the next surface modification. The etching process was terminated by rinsing several times with DI water until the pH of the wash solution became neutral.

In the final step, the embedded particles were recovered by dissolution of the fiber mats in an acetone/ethanol cosolvent (1:1 by volume), followed by centrifugal separation. Solvent washing and centrifugation were repeated four more times to complete the sample purification.

RESULTS AND DISCUSSION

As shown in Figure 1, the Janus particle preparation procedures were categorized into three distinct fabrication paths. The first procedure involved only one particle embedding and one surface silanization, producing Janus particles with two hemispherical surfaces, one of raw silica and one with amino functionality. Thermally manipulated particle embedding allowed the following CVD modifications to be restricted to only the exposed two-thirds, half, or one-third silica surfaces. Janus particles with two hemispheres with amino/silica ratios of 2:1, 1:1, and 1:2 were denoted as JP-2-1, JP-1-1, and JP-1-2, respectively. After labeling of the amino-enriched surfaces with Au NPs, transmission electron microscopy (TEM) imaging (Figure 2a,c) clearly distinguished functionalized hemispheres with the desired ratios.

Restricted by the curved particle surfaces, the uniformity and distribution of surface functionalities could not be directly determined by two-dimensional projection images such as SEM or TEM. Therefore, the degrees of colloid submergence and uniformity were used to quantify the surface-functionality contents. For the two-thirds- and half-embedded particles (samples JP-1-2 and JP-1-1, respectively), the SEM images shown in Figure 3b,c revealed their one-third and half outer hemispheres. The diameters of these outer hemispheres (D_{out}) were measured for statistical analysis. However, with the one-third-submerged particles, the outlines of the embedded edges were usually overshadowed by their own contours, as shown in SEM images. A

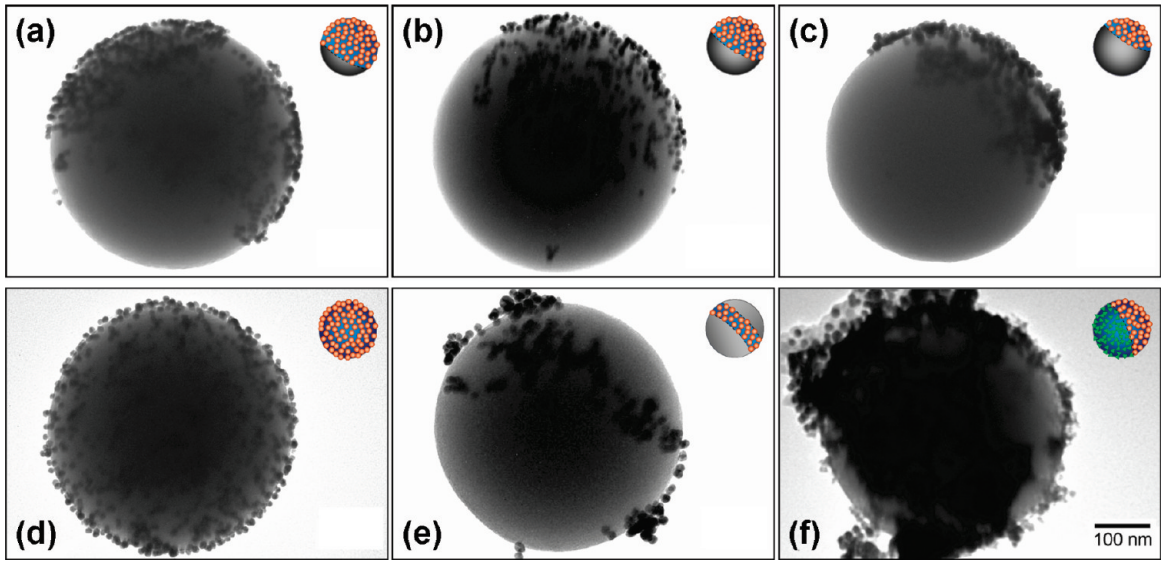

FIGURE 2. TEM images of (a) JP-2-1, (b) JP-1-1, (c) JP-1-2, (d) a fully silanized silica particle labeled with Au NPs, (e) a ternary particle, and (f) a bifunctionalized Janus particle. These images were purposely selected particles that were positioned with the particular angle.

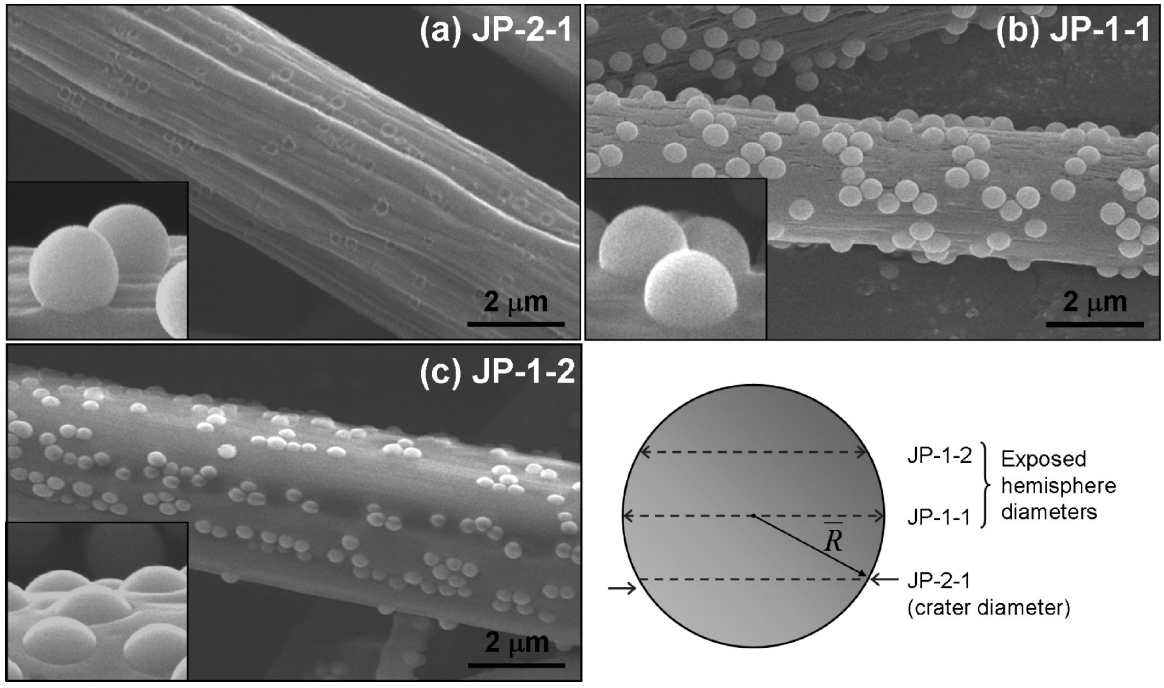

FIGURE 3. SEM images of electrospun polymer fibers with (a) craters after detachment of one-third-embedded silica particles, (b) half-embedded silica particles, and (c) two-thirds-embedded silica particles. The insets show the zoom-in images of embedded silica particles. The crater diameters (JP-2-1) and exposed hemisphere diameters (JP-1-1 and JP-1-2) were measured and statistically analyzed to determine particle-embedding uniformities.

special treatment of 10 min of sonication in an ice−water bath was applied to effectively remove the one-third-submerged particles from the polymer-fiber substrates. Figure 3a illustrates the craterlike holes on the fiber surfaces after the particles were detached. The diameters of these craters were also recorded and analyzed.

Because the silanized functionalities and the interfacial tension between silica and the polymer substrates were both correlated with spherical surface areas, the characteristic uniformities of these heterogeneous particles were represented by the distributions of their specific surface areas. For instance, the SEM images revealed that the average diameter ($\bar{D}$) of the precleaned silica particles was 450 nm. The diameters of 150 silica particles were measured and individually converted into their corresponding spherical surface areas for statistical analysis. The average surface area ($\bar{S}$) and standard deviation (S_{st}) were calculated to be 309 836 and 37 724 nm^2, respectively. The surface-based uniformity was then expressed as 1 − CV, where CV is the coefficient of variation given by CV = $S_{st}/\bar{S}$. As summarized in Table 1, the uniformity of the surface area of the precleaned silica particles was determined to be 87.8%.

Similarly, the outer-hemisphere diameters (D_{out}) of the embedded samples JP-1-2 and JP-1-1 (two-thirds- and half-

Table 1. Specific Diameters and Surface Characteristics of Janus and Ternary Particles

		specific surface area			surface characteristics	
sample no.	specific diameter (average, nm)	average (nm^2)	STD	uniformity (1 − CV, %)	amino-enriched area (%)	pI values (isoelectric point)
precleaned silica particle	450	619 672[a]	75 448	87.8	0 (100% silanol)	3.1
JP-2-1	303[b]	86 508[b]	19 683	81.0	83.6	4.5
JP-1-1	450[c]	327 505[c]	39 970	86.8	51.6	6.2
JP-1-2	306[c]	104 315[c]	17 353	83.3	13.6	7.2
ternary		466 058[d]	77 357	83.4	69.9	7.3
amino silica					100	8.6

[a] The surface area of the sphere. [b] The crater diameter and the calculated crater surface area. [c] The exposed hemisphere diameters and surface areas. [d] The calculated belt surface area of the ternary particles.

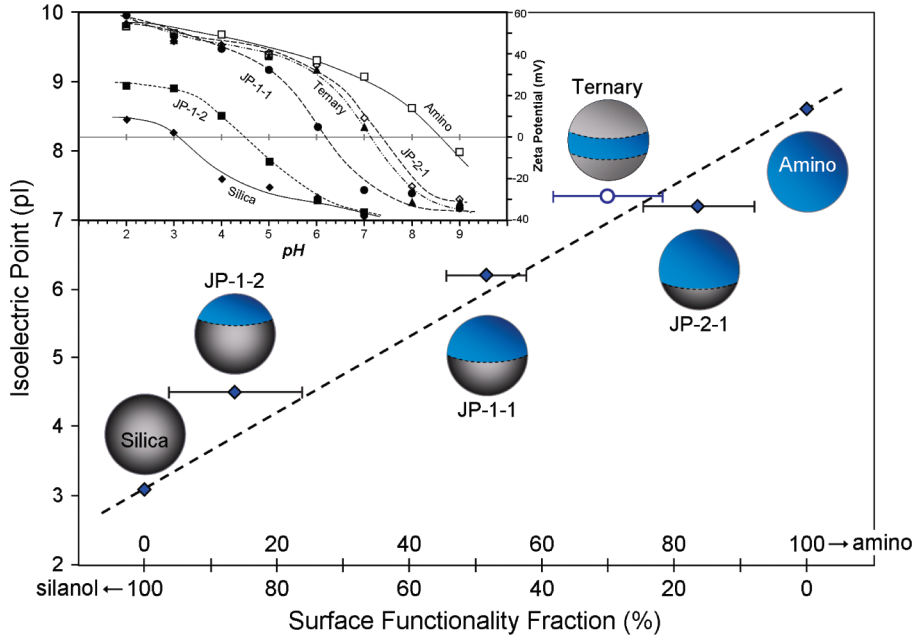

FIGURE 4. Isoelectric points of all particles revealing the linear proportionality to the amino/silanol surface-functionality fractions. Error bars represent the corresponding uniformities of specific surface areas. The inset illustrates the isotherms of electrophoretic mobility vs pH.

submerged, respectively) were converted into their exposed surface areas. Statistical analysis of 150 particles determined the average surface areas and the corresponding standard deviations (details in Table 1). The uniformities of the exposed hemispheres of the JP-1-2 and JP-1-1 particles were determined to be 83.4% and 86.8%, respectively. For sample JP-2-1 (one-third-submerged), the uniformity calculation relied instead on the crater diameters, as previously described. The crater diameters demarcated the original contact surface areas between the detached particles and fiber substrates. On the basis of the analysis of 150 crater diameters, the surface uniformity of the JP-2-1 particles was determined to be 81.0%. Interestingly, the surface-area-based uniformities of these three Janus samples were all within the range of 81−88%, similar to that of the precleaned silica particles. These results indicated that the "built-in" uniformity of the particle-embedding process at a given temperature is greater than 80%.

Table 1 also lists the isoelectric points (pI) of these particles as determined by ζ-potential measurements. The pI values of the precleaned and 3-APTMS-functionalized silica particles were 3.1 and 8.6, respectively, representing the pH values at which the silanol and amino groups on the silica surfaces carried no net electrical charges. Without NP labelers, the ζ-potential profiles of amino-functionalized JP-2-1, JP-1-1, and JP-1-2 particles revealed that their pI values were 4.5, 6.2, and 7.2, respectively. Considering that the pI of a Janus particle results from the balance between its surface amino and silanol groups, the pI value should also be proportional to the ratio of the silanol and amino hemispherical surfaces. Figure 4 presents the linear relationship between these pI values and the amino or silanol surface-functionality fractions obtained from the previous embedding investigations.

The fabrication path II in Figure 1 illustrates the procedure used to produce ternary particles. The procedure consists of two steps of particle embedding, one surface-modification process, and one surface-etching process. Similar to the fabrication of sample JP-2-1, the one-third-embedded silica particles were first treated by CVD silanization and then by Au NP labeling. A second isothermal treatment was applied at the higher temperature of 150 °C for the supplementary embedding that buried the particle midsection and protected it from chemical or physical modification. The remaining

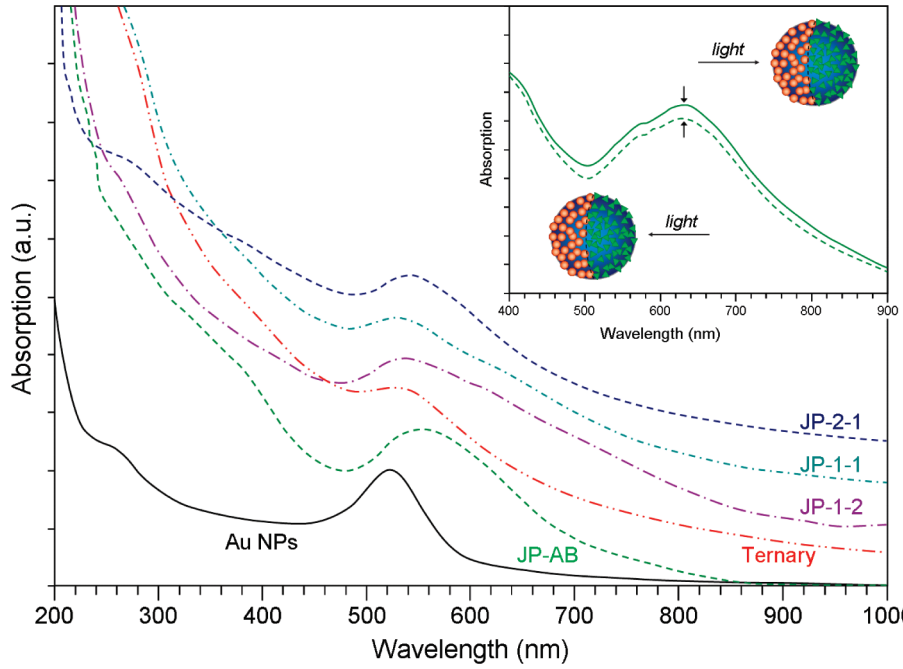

FIGURE 5. UV−vis spectra of an aqueous Au NP suspension (bottom) and silica particles labeled with Au NPs. The inset shows two spectra of the PMMA/JP−AB-coated layers measured from opposite directions.

one-third-exposed hemisphere (the upper cap) was then etched with a basic solution to remove the aminosilane moieties and Au NPs from the silica surface. Because of the insolubility of PMMA and P4VP in a basic aqueous solution, the etching formula had no effect on the fiber scaffold or on the silica surface functionalities embedded underneath. After particle recovery and routine purification, the TEM image (Figure 2e) captured the Au-NP-labeled "belt" of a ternary particle. In a separate fabrication, amino-functionalized ternary particles without Au NP labeling were also prepared for ζ-potential measurement. Their pI value of about 7.3 was compared with the 69.9% amino-enriched surface fraction based on the calculations of the degrees and uniformities of the surface-area coverages of the one-third- and two-thirds-submerged particles. As shown in Figure 4, the surface amino/silanol ratio of the ternary particles showed a linear correlation with the zero-charge pH value. On the basis of the embedding uniformities of the one-third- and two-thirds-submerged particles, the surface-functionality distribution of ternary particles was also estimated to have a minimum uniformity of 80%.

Fabrication path III resulted in the preparation of bifunctionalized Janus particles. Prior to adsorption of the silica particles onto the fiber surfaces, the sphere surfaces were fully silanized with 3-APTMS in a liquid-phase reaction, followed by labeling with Au NPs (see the TEM image in Figure 2d). The half-embedding of these prefunctionalized silica particles was carried out at 120 °C. The exposed aminosilane coatings and Au NPs on the upper hemispheres were then etched with the basic solution as previously described. Subsequently, the introduction of a second CVD silanization generated fresh amino-enriched hemispherical surfaces that were relabeled with citrate-modified Fe_3O_4 NPs. Figure 2f shows the TEM image of a bifunctionalized Janus particle (JP−AB) with Au NPs on the right side and aggregated Fe_3O_4 NPs on the left.

Figure 5 presents UV−vis spectra of aqueous suspensions of samples JS-2-1, JS-1-1, JS-1-2, and JP−AB. Au NPs attached to these Janus and ternary silica particles had SPR absorption bands at about 520 nm similar to those of the original Au NPs in aqueous suspension. The bifunctionalized JP−AB suspension exhibited a red-shifted SPR absorption at about 560 nm. In a sample vial containing 15 mL of an aqueous suspension of JP−AB particles, the anisotropic SPR responses were also manipulated by a magnetic stirrer. As the stirrer was turned on, the purple-reddish solution immediately glimmered under the ambient light (29). Higher stirring rates accelerated the glimmering, whereas the liquid surface remained quiescent. The glimmering instantly ceased upon when the stirrer was turned off, and the solution returned to its original appearance with no trace of turbulence. These observations indicated that the dynamic magnetic field rapidly interrupted the random rotation of suspended JP−AB particles, overcoming the momentum of Brownian motion.

In a separate experiment, an MEK suspension of PMMA and JP−AB particles was cast on a quartz slide. A magnet was placed underneath to align the randomly oriented JP−AB particles. Just before complete solvent evaporation, the PMMA/JP−AB layer was carefully sandwiched by a second quartz slide. Complete solvent removal and PMMA/JP−AB solidification were ensured by keeping the sandwiched film and the underlying magnet in a vacuum chamber at room temperature overnight. This sandwiched PMMA/JP−AB layer appeared identical from either side. However, the transmission UV−vis spectra of this sandwiched layer taken from two opposite directions revealed considerable variation in the SPR wavelengths and intensities (see the inset spectra in Figure 5). First, the concentrated JP−AB

particles in the solidified PMMA layer had an SPR band centered at 630 nm, much higher than the 560 nm band of the same sample suspended in an aqueous solution. Additionally, the intensity of the SPR absorption of this sandwiched layer decreased more than 6% when measured in two opposite directions. Presumably, this difference is because of the greater SPR absorption when the Au NP hemispheres of JP−AB particles mostly faced the incident light, whereas the incident light from the opposite direction had fewer Au NPs in its light path.

CONCLUSIONS

In this study, asymmetric Janus and ternary silica particles with an average diameter of 450 nm were successfully fabricated via sequentially arranged particle-embedding and surface-modification processes. Temperature-dependent particle embedding on polymer-fiber substrates allowed for the manipulation of the surface areas of the exposed hemispheres, and the desired chemical functionalities could then be attached or etched away. Statistical analyses of the degrees of particle submergence revealed consistent and uniform embedding behavior. The functionality distributions on these submicrometer sphere surfaces were determined to be more than 80% uniform. The surface amino/silanol ratios of these particles were also found to be linearly proportional to their isoelectric points. Bifunctionalized Janus particles labeled with Au and Fe_3O_4 NPs on opposing hemispherical surfaces were fabricated to demonstrate the interference of anisotropic SPR by a magnetic field.

Acknowledgment. The authors gratefully acknowledge the Center for Micro/Nano Science and Technology at the National Cheng Kung University for providing facilities and the National Science Council, Taiwan, for its financial support (Grants NSC 97-2221-E-006-115 and NSC 98-3114-E-006-010).

REFERENCES AND NOTES

(1) de Gennes, P.-G. *Rev. Mod. Phys.* **1992**, *64*, 645–648.
(2) Perro, A.; Reculusa, S.; Ravaine, S.; Bourgeat-Lami, E.; Duguet, E. *J. Mater. Chem.* **2005**, *15*, 3745–3760.
(3) Roh, K.-H.; Martin, D. C.; Lahann, J. *Nat. Mater.* **2005**, *4*, 759–763.
(4) Cayre, O.; Paunov, V. N.; Velev, O. D. *Chem. Commun.* **2003**, 2296–2297.
(5) Paunov, V. N.; Cayre, O. J. *Adv. Mater.* **2004**, *16*, 788–791.
(6) Cui, J.-Q.; Kretzschmar, I. *Langmuir* **2006**, *22*, 8281–8284.
(7) Hong, L.; Jiang, S.; Granick, S. *Langmuir* **2006**, *22*, 9495–9499.
(8) Jiang, S.; Schultz, M. J.; Chen, Q.; Moore, J. S.; Granick, S. *Langmuir* **2008**, *24*, 10073–10077.
(9) Erhardt, R.; Boeker, A.; Zettl, H.; Kaya, H.; Pyckhout-Hintzen, W.; Krausch, G.; Abetz, V.; Mueller, A. H. E. *Macromolecules* **2001**, *34*, 1069–1075.
(10) Charlaganov, M.; Borisov, O. V.; Leermakers, F. A. M. *Macromolecules* **2008**, *41*, 3668–3677.
(11) Voets, I. K.; Fokkink, R.; Hellweg, T.; King, S. M.; Waard, P. D.; De Keizer, A.; Cohen Stuart, M. A. *Soft Matter* **2009**, *5*, 999–1005.
(12) Pradhan, S.; Xu, L.-P.; Chen, S. *Adv. Funct. Mater.* **2007**, *17*, 2385–2392.
(13) Feng, X.; Taton, D.; Ibarboure, E.; Chaikof, E. L.; Gnanou, Y. *J. Am. Chem. Soc.* **2008**, *130*, 11662–11676.
(14) Nisisako, T.; Torii, T.; Takahashi, T.; Takizawa, Y. *Adv. Mater.* **2006**, *18*, 1152–1156.
(15) Graham-Rowe, D. *Nat. Photonics* **2007**, *1*, 248–251.
(16) Zhao, N.; Gao, M. *Adv. Mater.* **2009**, *21*, 184–187.
(17) Dyab, A. K. F.; Ozmen, M.; Ersoz, M.; Paunov, V. N. *J. Mater. Chem.* **2009**, *19*, 3475–3481.
(18) Isojima, T.; Suh, S. K.; Vander Sande, J. B.; Hatton, T. A. *Langmuir* **2009**, *25*, 8292–8298.
(19) Roh, K.-H.; Yoshida, M.; Lahann, J. *Langmuir* **2007**, *23*, 5683–5688.
(20) Glotzer, S. C. *Science* **2004**, *306*, 419–420.
(21) Hong, L.; Cacciuto, A.; Luijten, E.; Granick, S. *Nano Lett.* **2006**, *6*, 2510–2514.
(22) Yoshida, M.; Roh, K.-H.; Lahann, J. *Biomaterials* **2007**, *28*, 2446–2456.
(23) Isojima, T.; Lattuada, M.; Vander Sande, J. B.; Hatton, T. A. *ACS Nano* **2008**, *2*, 1799–1806.
(24) Kang, S.; Suci, P. A.; Broomell, C. C.; Iwahori, K.; Kobayashi, M.; Yamashita, I.; Young, M.; Douglas, T. *Nano Lett.* **2009**, *9*, 2360–2366.
(25) Nie, Z.; Li, W.; Seo, M.; Xu, S.; Kumacheva, E. *J. Am. Chem. Soc.* **2006**, *128*, 9408–9412.
(26) Ho, C.-C.; Chen, W.-S.; Shie, T.-Y.; Lin, J.-N.; Kuo, C. *Langmuir* **2008**, *24*, 5663–5666.
(27) Ye, S.; Carroll, R. L. *ACS Appl. Mater. Interfaces* **2010**, *2*, 616–620.
(28) Bee, A.; Massart, R.; Neveu, S. *J. Magn. Magn. Mater.* **1995**, *149*, 6–9.
(29) See http://www.youtube.com/watch?v=EhwNlYld5C0 for a video of a magnetically manipulated JP−AB aqueous suspension.

AM1006589